Clark Lake Experience and SIRA

Mukul Kundu

May 13-14, 2003

People involved in CLRO solar work

Borrego Springs

- Peter Turner
- Alex Szabo
- Barbara
- Jim Rickard
- J C Pigg
- Brett Hamlet
- H Sawant

College Park

- Tom Gergely
- Peter Jackson
- Ed Schmahl
- Steve White
- Golla Thejappa
- Nat Gopalswamy
- Z Wang-Student

Clark Lake Array

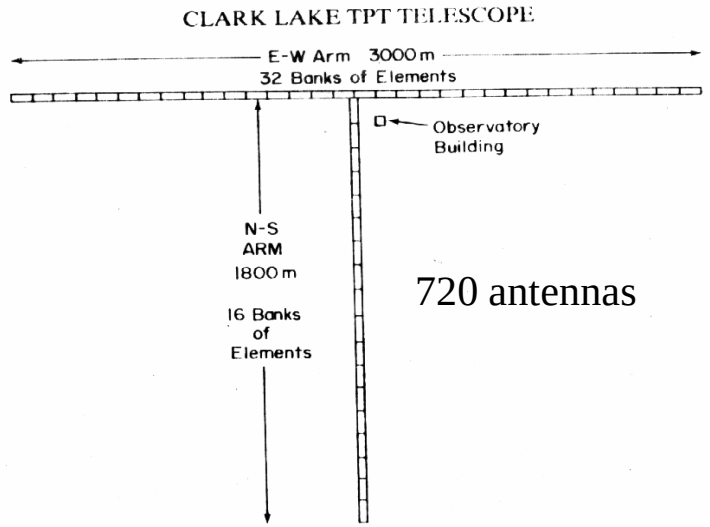

Freq range 20-125 MHz (38,50,74 MHz often used); Ang.res ~2.’5 at 120 MHz, ~15’ at 20; Sensitivity ~1Jy; Dynamic range 100:1 at 50 MHz; 1 sec time res

First map of the Sun

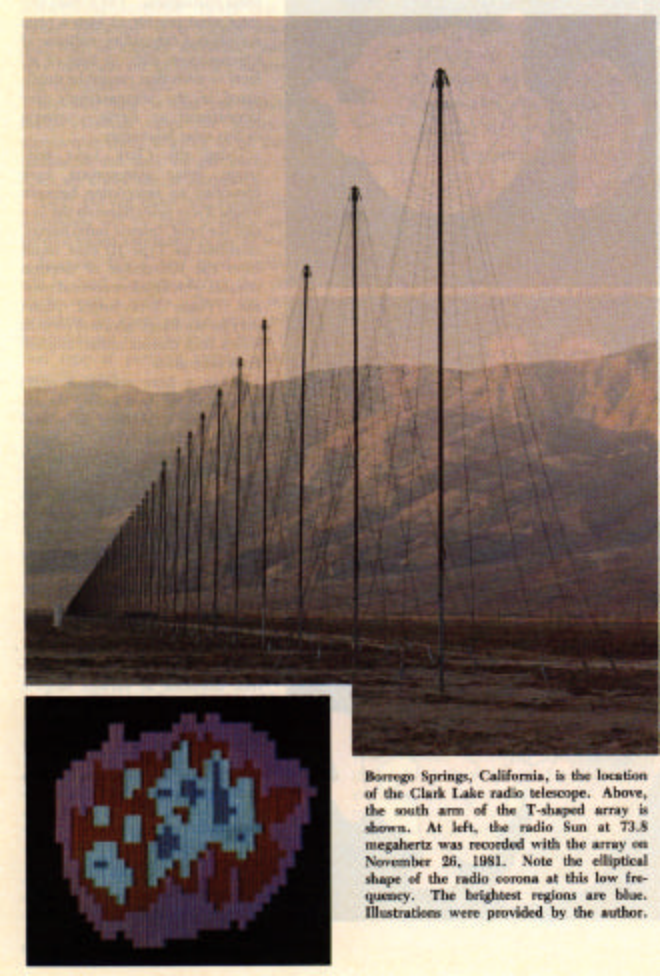

Borrego Springs, California, is the location of the Clark Lake radio telescope. Above, the south arm of the T-shaped array is shown. At left, the radio Sun at 73.8 megahertz was recorded with the array on November 26, 1981. Note the elliptical shape of the radio corona at this low frequency. The brightest regions are blue. Illustrations were provided by the author.

Solar maps at 3 frequencies, showing elongated features

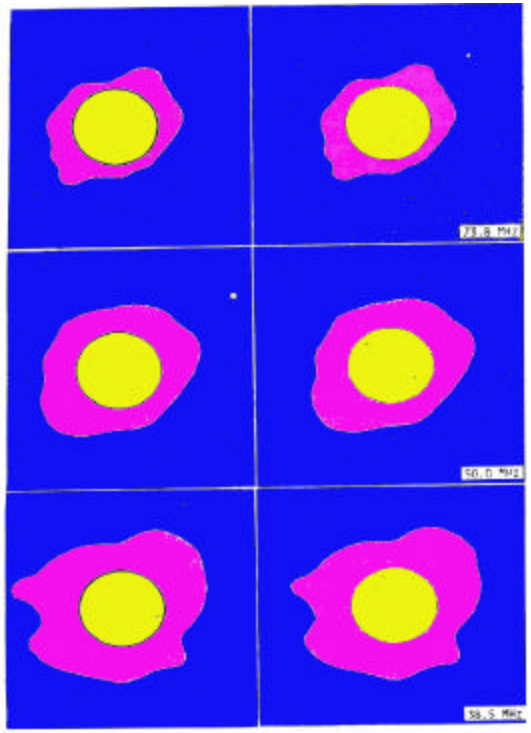

Figure 1. Left: Radio maps of the Sun at 73.8, 50 and 38.5 MHz (from top to bottom). Right: Same maps with central portion equivalent to optical disk blocked out.

Showing plasma levels at different frequencies

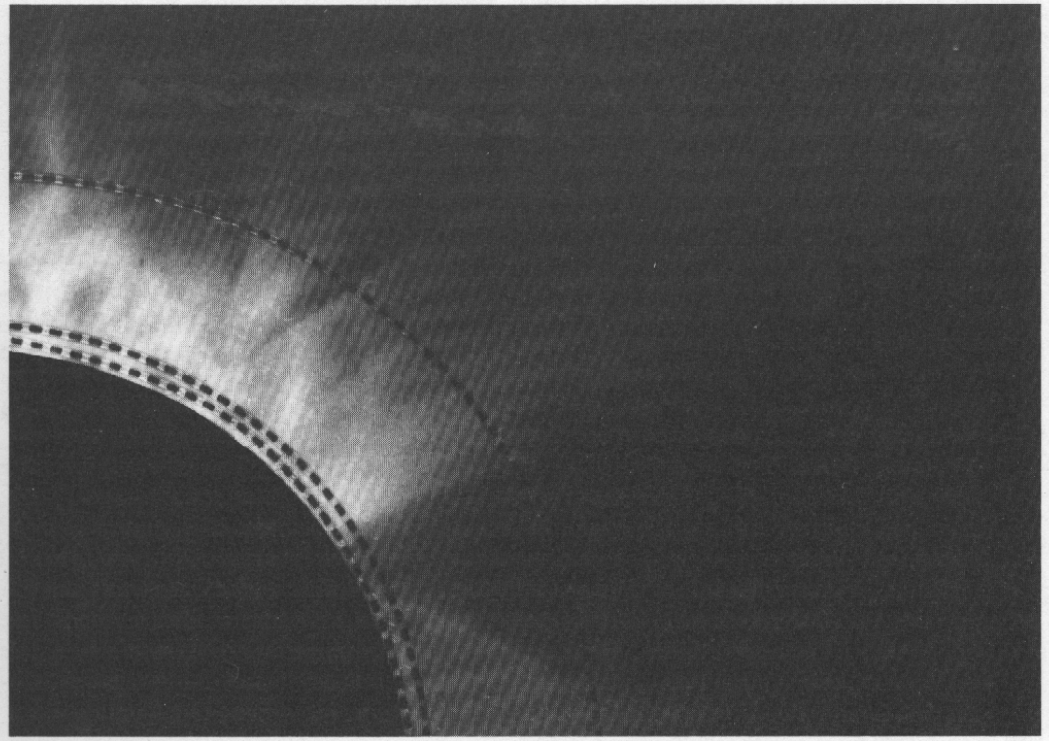

Coronal loops and streamers appear in this photograph of the total solar eclipse of February 16, 1980, made by the High Altitude Observatory and Southwestern at Memphis. The dashed arcs indicate the approximate levels where radio emission at different wavelengths originates. Moving outwards from the Sun the domains correspond to 6 cm (5,000 GHz), 20 cm (1,400 GHz), and 3m (100 MHz).

Coronal Streamers on Solwind Coronagraph and Type III Bursts

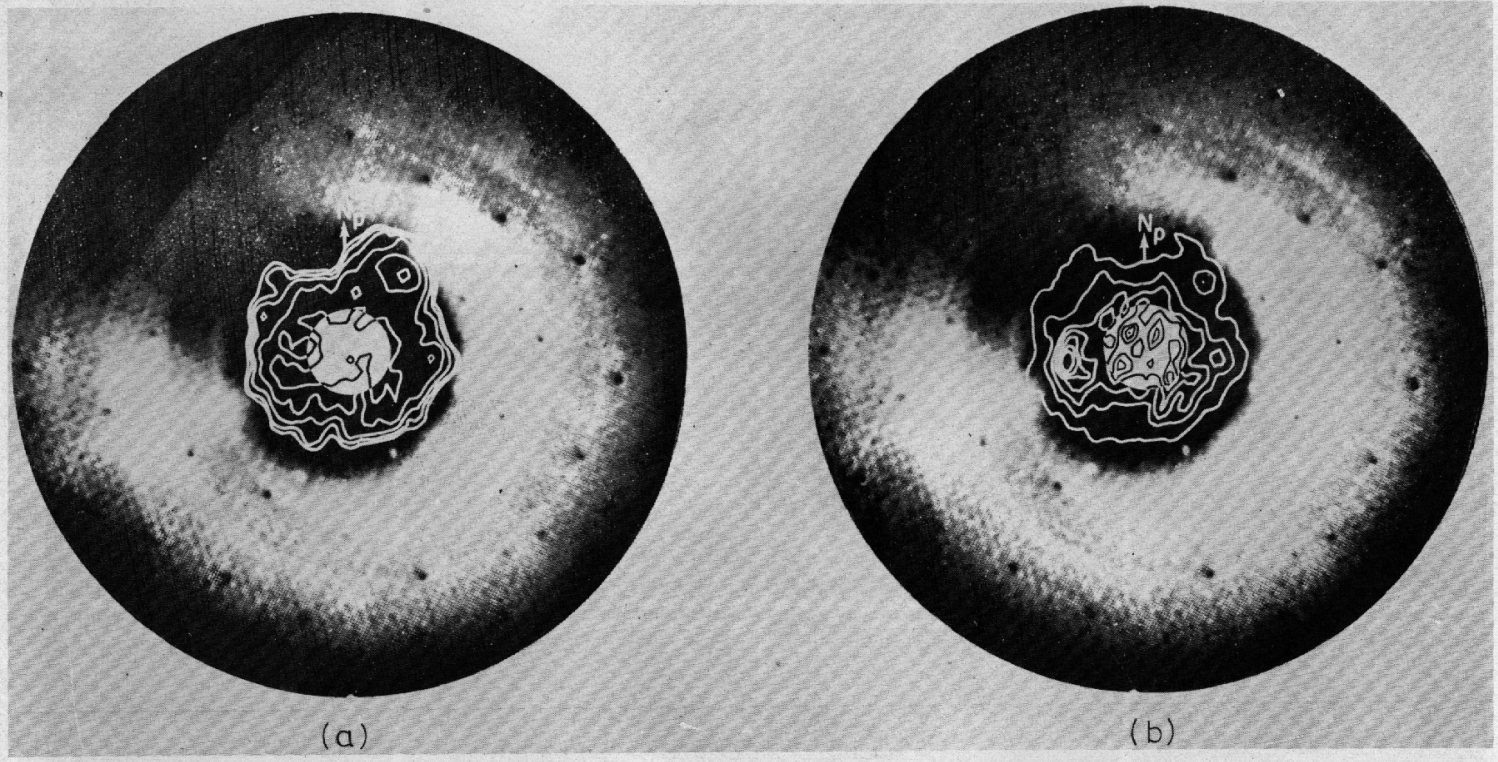

Fig. 5a,b—Radioheliograph images showing weak type III bursts superposed on white light photographs of the corona obtained by the coronagraph aboard the P78-1 satellite (a, b) and the HAO's coronagraph/polarimeter (C/P) aboard SMM satellite (c). The spatial scale of both radio and optical pictures is identical, the white circle at the centre is the size of the optical sun. Note the close correspondence of the centroid of the radio sources and the white-light streamers. In (a) logarithmic contours and in (b) linear contours are used for weak type III bursts observed at 73.8 MHz on 26 Nov. 1981; in (c) linear contours at 73.8, 50 and 38.5 MHz (top, middle and bottom rows respectively) are shown for type III bursts observed on 27 July 1985 (Column 1), 12 Sep. (Column 2), and 17 Sep. (Column 3).

Coronal density from Solwind coronagraph

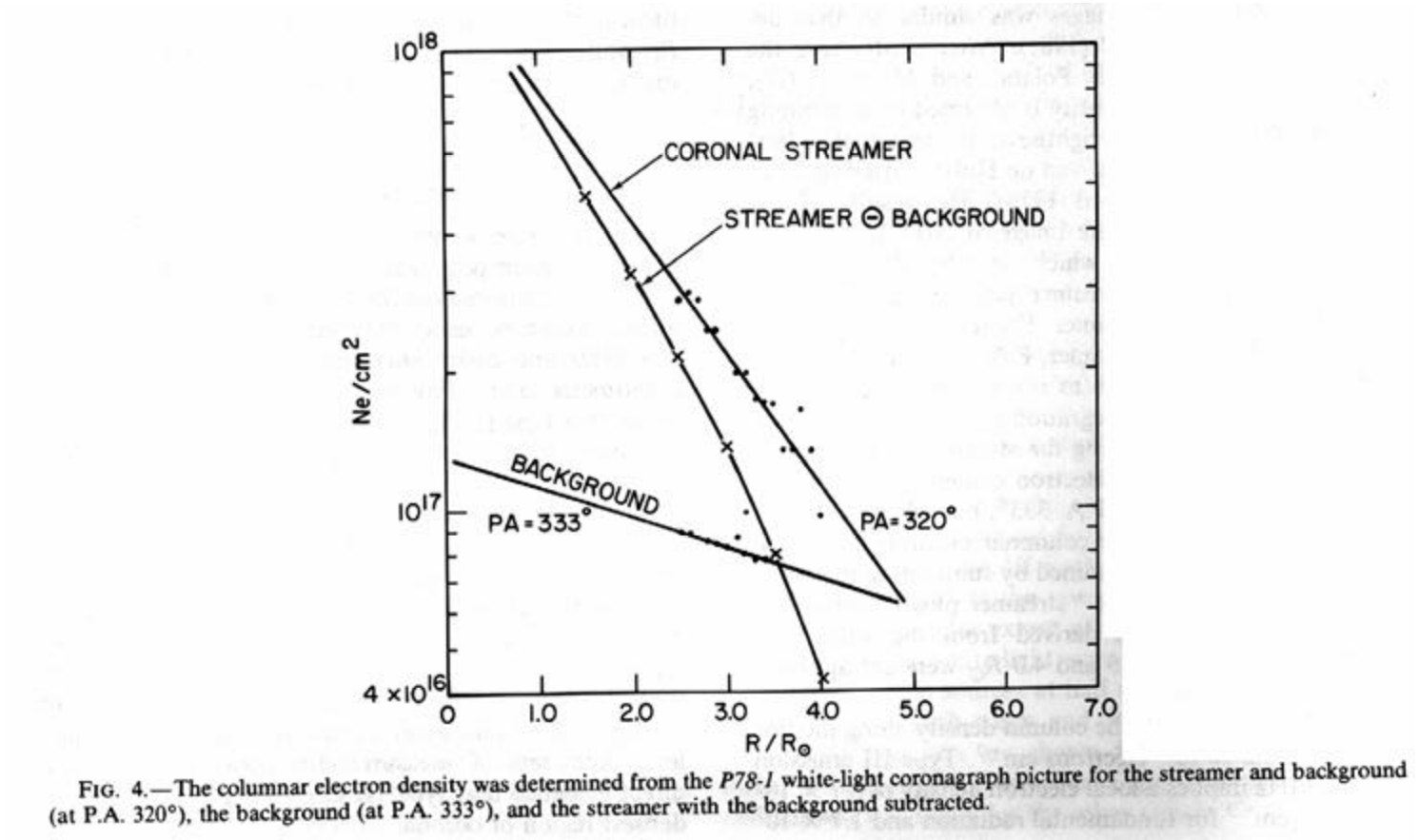

FIG. 4.—The columnar electron density was determined from the *P78-1* white-light coronagraph picture for the streamer and background (at P.A. 320°), the background (at P.A. 333°), and the streamer with the background subtracted.

Weak TypeIII bursts in Coronal streamers and coronal density measurements

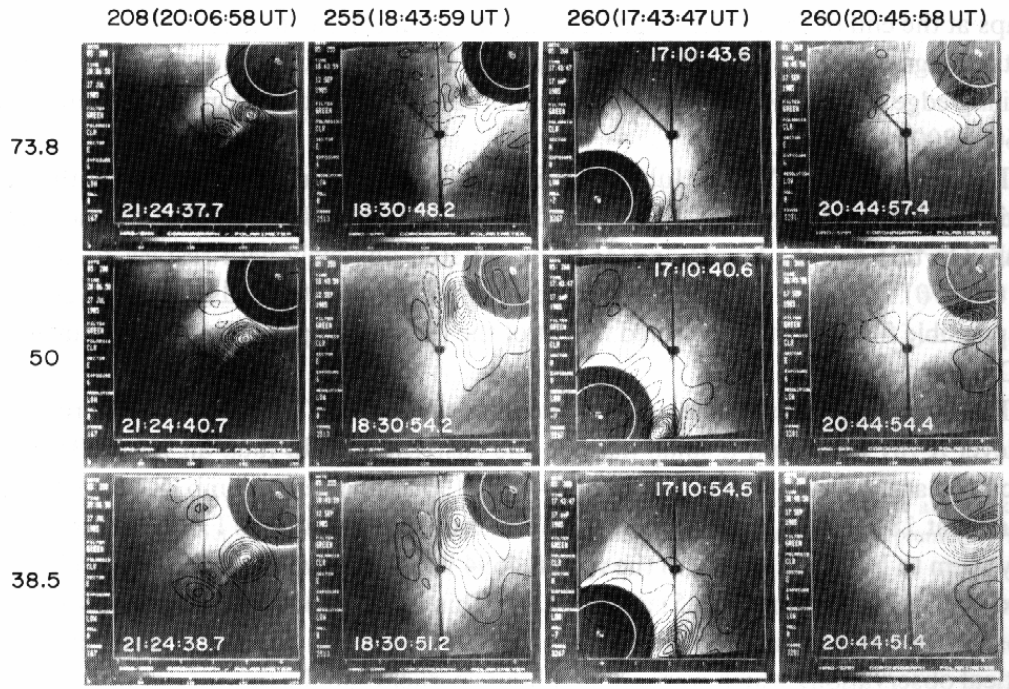

Fig. 6. Superposition of type III bursts at 73.8, 50.0, and 38.5 MHz on HAO–C/P picture of coronal streamers for DOY 208, 255, and 260. The time of C/P picture is indicated on each column. The time of the type III burst is indicated in the corners of the figures.

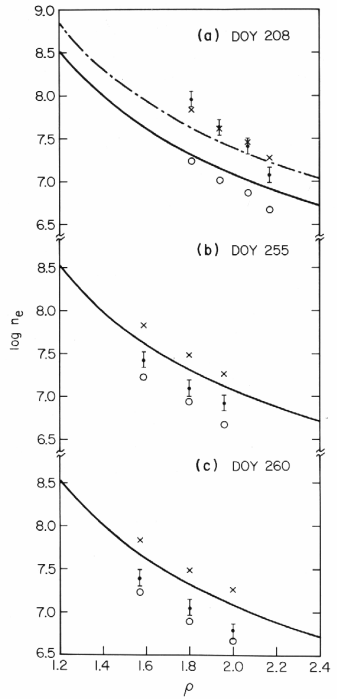

Fig. 7. The plot of coronal electron density (n_e) as a function of radial distance ρ (in units of solar radius) for (a) DOY 208, (b) DOY 255, and (c) DOY 260. The solid and dot-dashed curves are due to Newkirk's streamer and 2× Newkirk's streamer models, respectively. × and ○ correspond to electron densities obtained by assuming fundamental and harmonic plasma emission, respectively. ⧳ represent electron density obtained from HAO SMM–C/P.

Coronal Streamers in radio in all their glory (with Solwind in white light) and 3-D Structures

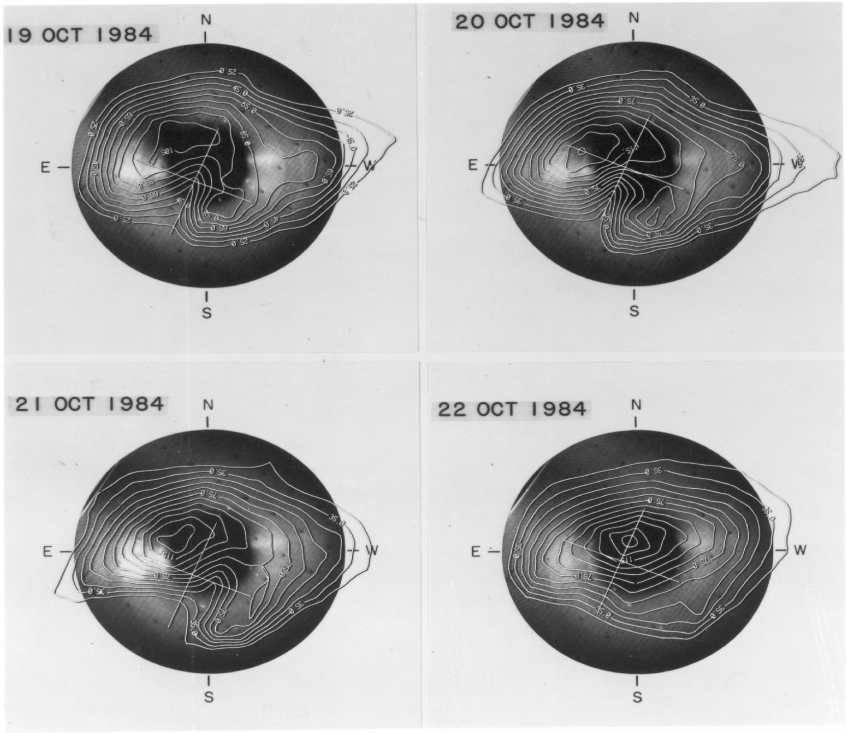

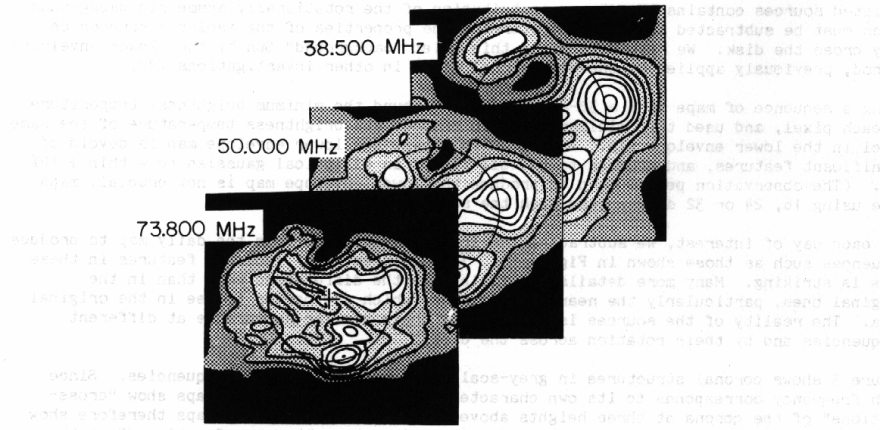

Fig. 3 Difference maps in grey-scale showing the "sectioning" of the coronal forms (holes and streamers) at the plasma levels characteristic of each frequency.

Coronal Holes and their evolution at three different frequencies

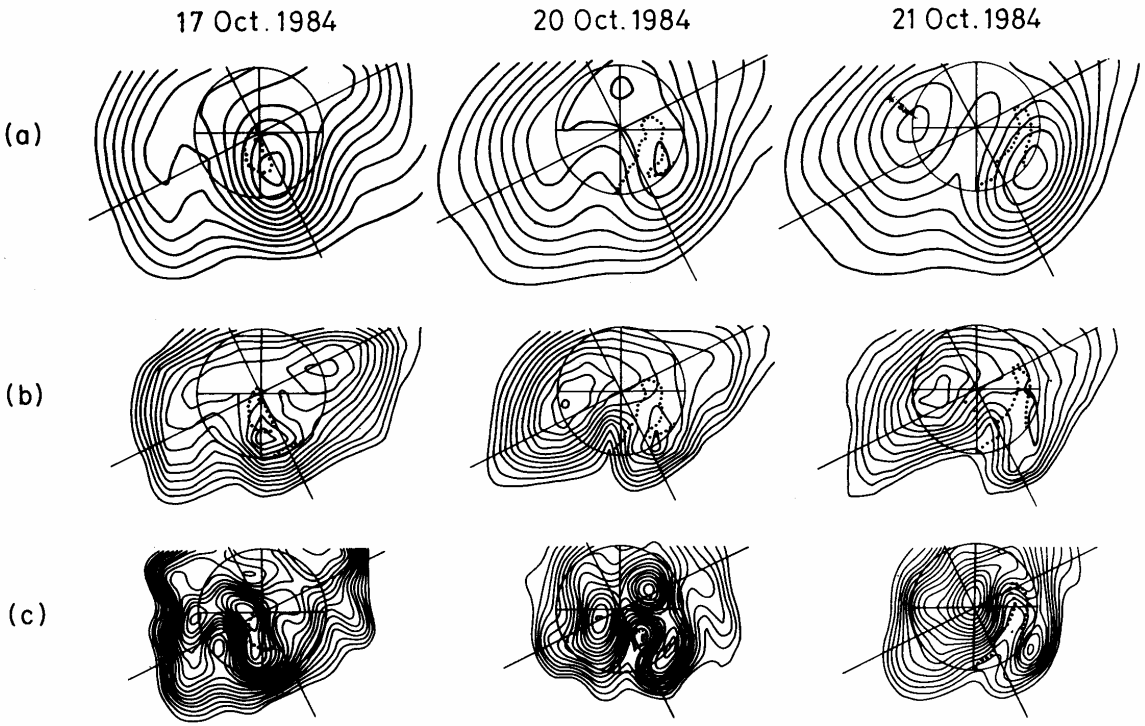

Fig. 2 — CLRO maps on 17, 20 and 21 Oct. 1984 showing the coronal hole at (a) 30.9, (b) 50 and (c) 73.8 MHz. The 10830 Å hole boundary is shown by the dotted curves on each of the radio maps. On 20 and 21 Oct., the correspondence is excellent between the 73.8 MHz contours and 10830 Å, which may mean that at this frequency the hole extends down close to the chromospheric level. However, the hole appears displaced eastward as one moves to lower frequencies (greater heights), indicating a backward bending of the hole.

Microbursts at low frequencies: First Measurements- they seem to be type IIIs

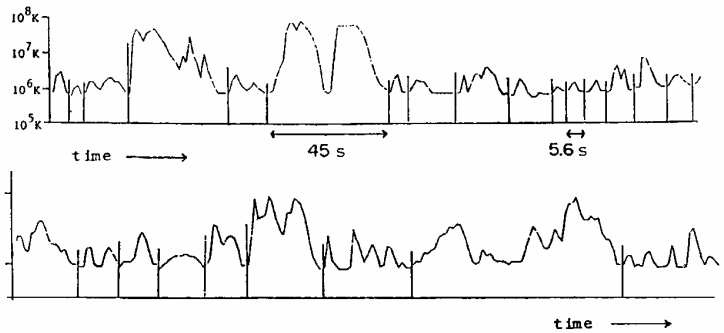

Fig. 6 — A compilation of the peak brightness temperature measurements of the sun at 50 MHz as a function of time for the periods during which microbursts occurred during several hours on 23 Mar. 1985. Breaks in the record are indicated by vertical lines. Consecutive points are 1.4 s apart. The vertical scale is logarithmic. The instrument saturates for brightness temperatures in excess of 10^8 K.

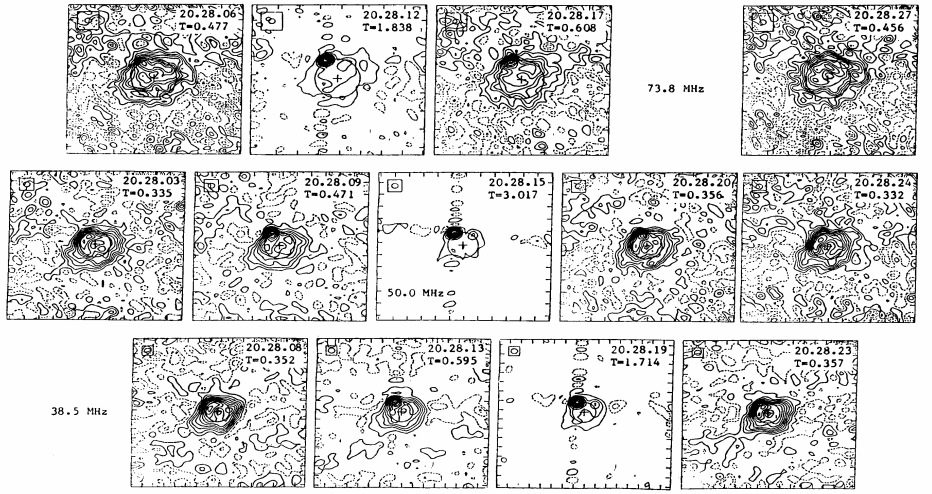

Fig. 8—Clark Lake maps showing the evolution of a microburst (15 Aug. 1985) at three frequencies. The maps on the top line are at 74 MHz. The time of each map and the peak brightness temperature in units of 10^8 K are indicated in the inset in the upper right corner. The maps on the middle row are at 50 MHz, and those on the bottom row are at 39 MHz. Time proceeds from left to right.

Low Freq microbursts originate from different regions: Also high T_B's

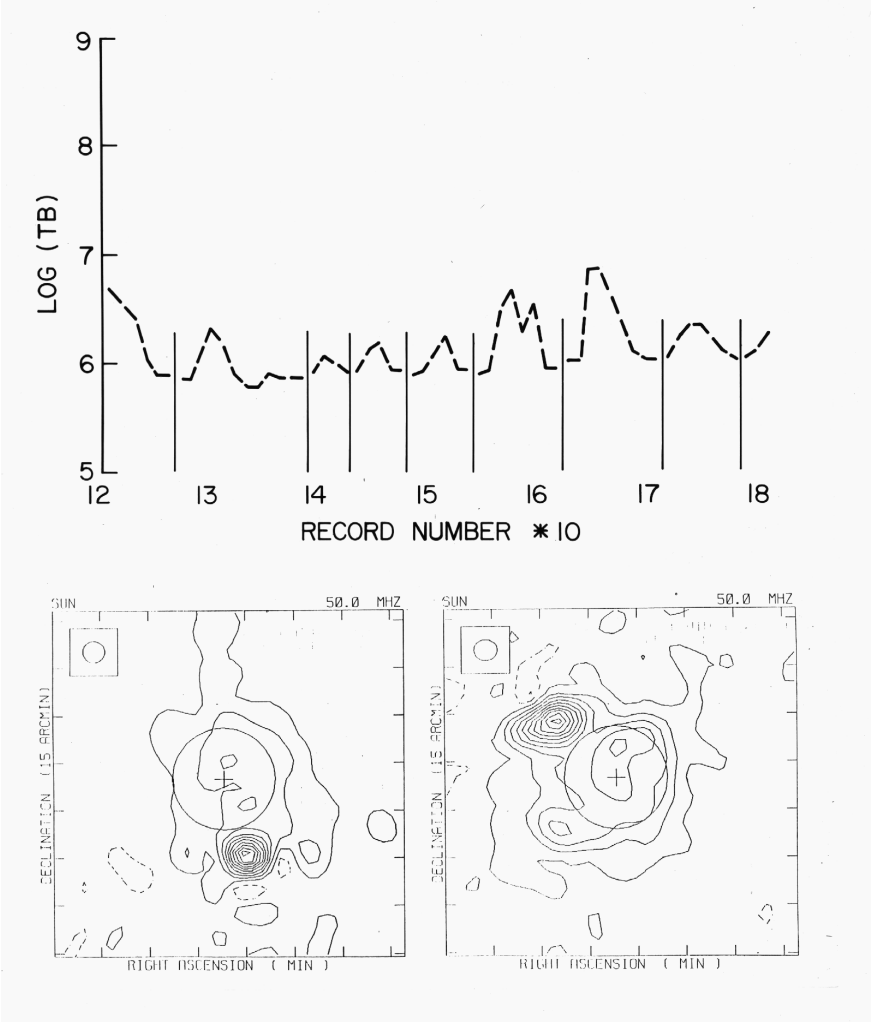

A normal Type III and its evolution at 50MHz in 8 seconds

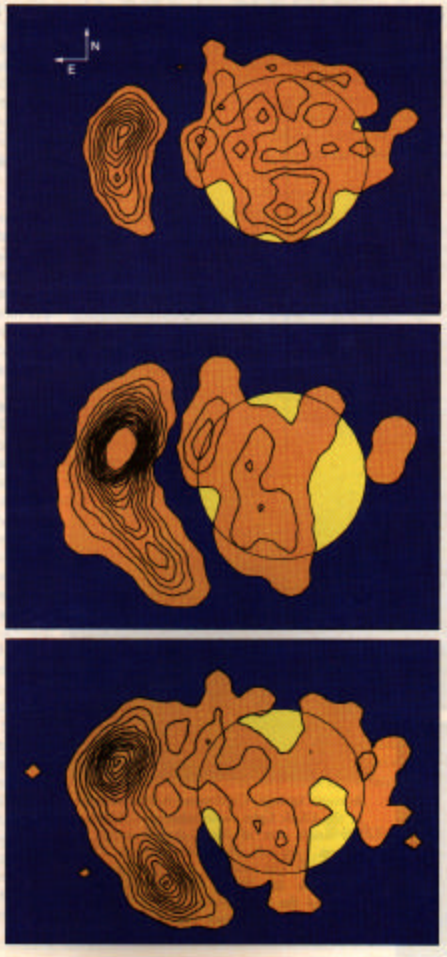

and streams of electrons. Fundamental physical processes shape these phenomena. The corona and solar wind provide us with a plasma-physics laboratory millions of kilometers in size. A host of effects — ones that cannot be duplicated in the comparatively tiny laboratories on Earth — operate in this solar laboratory.

Using the Clark Lake telescope, solar astronomers have identified an association between bright X-ray point flares on the Sun and the brief, intense radio bursts, classified as Type III that result from the interaction of electron streams with ambient coronal plasma. These X-ray-bright points may be the flares' simplest form in which such plasma radiation processes take place.

When a flare occurs, a radio image can be recorded by the array at the same time as photographs are being taken. Comparisons of the radio and optical images are most instructive. They tell us that flares exploding on the Sun's surface emit electron streams that penetrate the corona, propagate along coronal streamers and cause Type III radio bursts. In the future it may be possible to use on a routine basis rapid-sequence measurements of Type III bursts at different frequencies to derive electron densities at various heights in the Sun's atmosphere.

Other solar observations at Clark Lake involve the violent

Left: **A solar burst, resembling one of Type III but much weaker, develops on July 5, 1982, in these Clark Lake radioheliograms. The first two views were made two seconds apart, the second and third views six seconds apart. The double structure in the third radioheliogram may indicate loop activity high in the corona.**

Different Types of Bursts at meter-decameter wavelengths

Type III

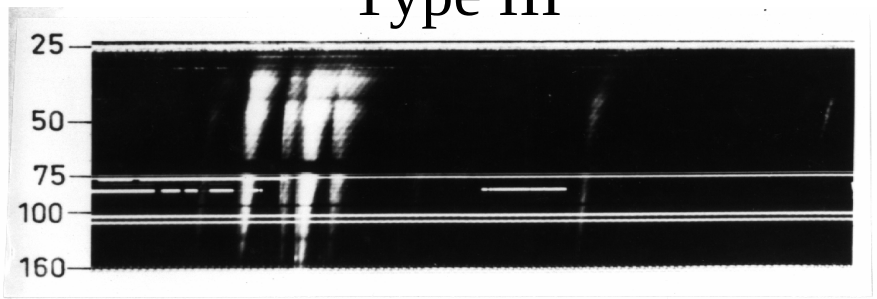

Type II

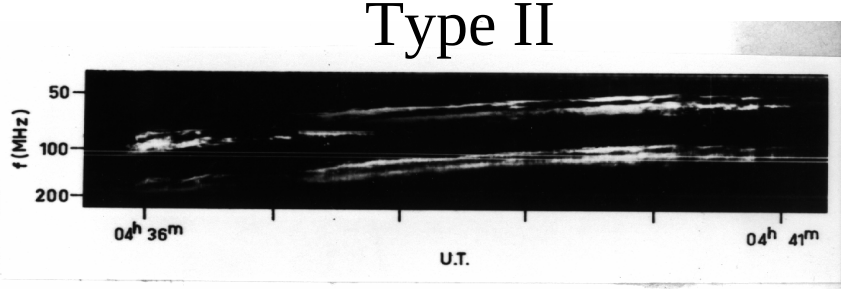

Type IV

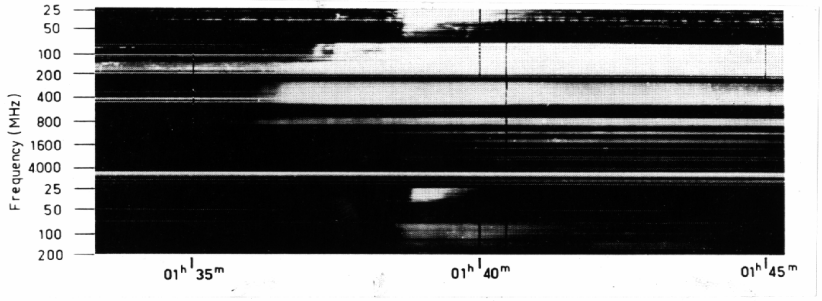

Type IV

A slow typeIV associated with Streamer disruption event

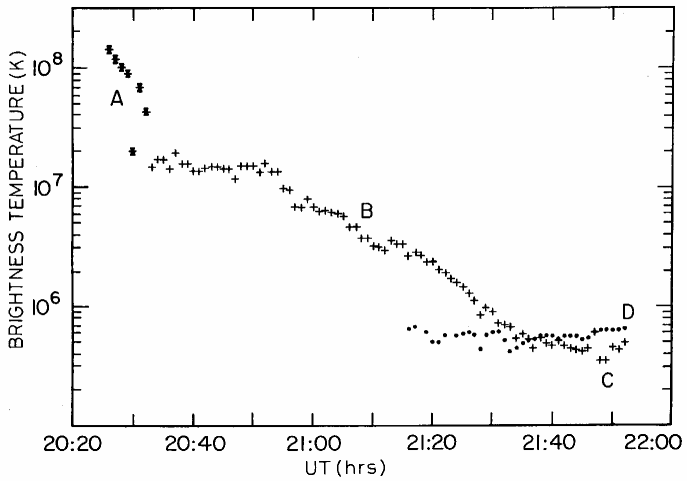

Fig. 10 — Brightness temperature plotted as a function of time for the type II and various phases of the type IV event

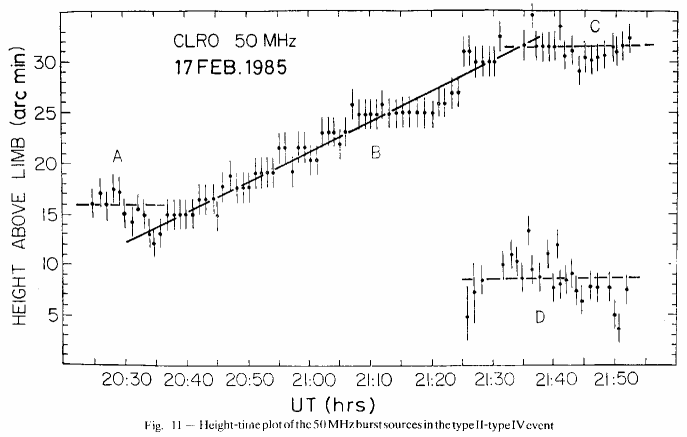

Fig. 11 — Height-time plot of the 50 MHz burst sources in the type II-type IV event

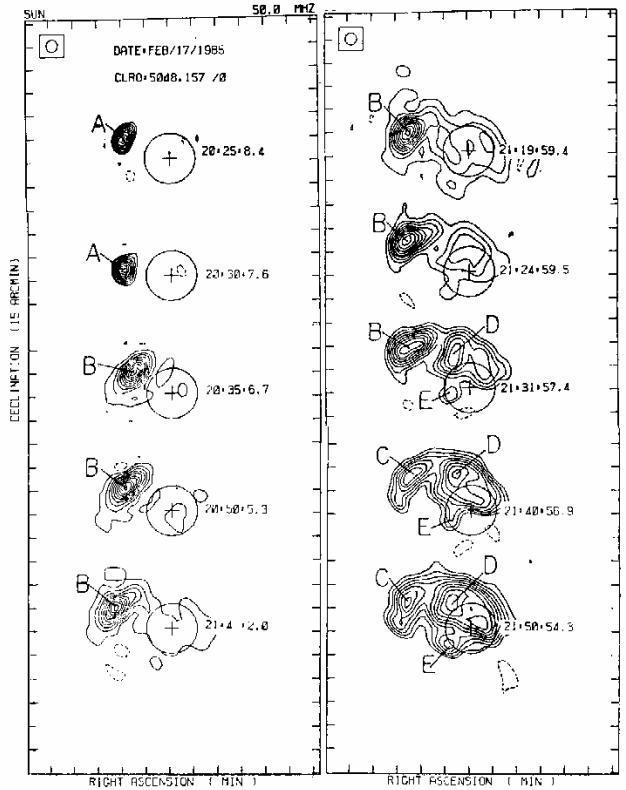

Fig. 1. Snapshot (0.6 s) maps of the Sun at 50 MHz, showing the evolution of the type II–type IV event associated with a coronal streamer disruption event.

The Slow Type IV associated with a CME (Streamer Blow out type)

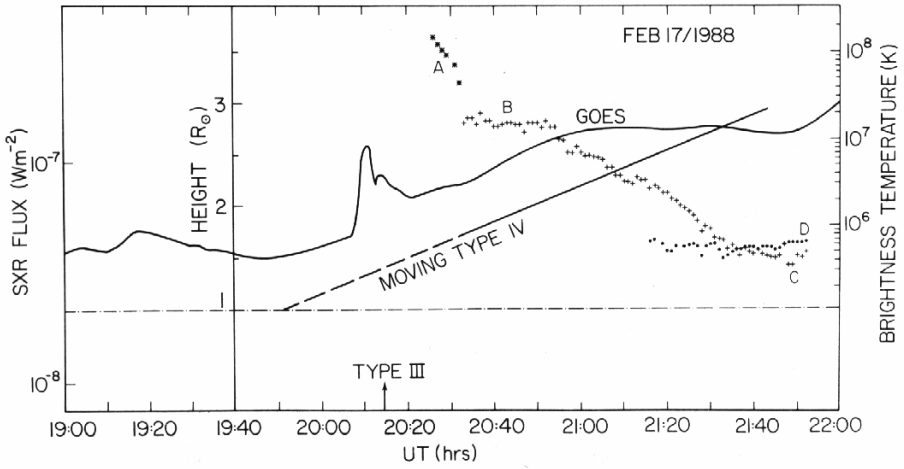

FIG. 2.—Chronological summary of various activities: light curve soft X-rays (*GOES* 1–8 Å); brightness temperature variation of type II (A), moving type IV (B, C), and stationary type IV bursts (D); height-time plot of moving type IV burst. The time of type III burst is marked.

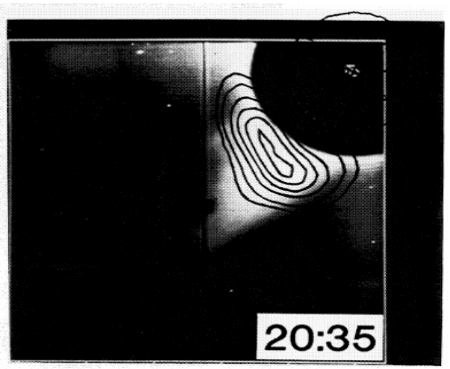

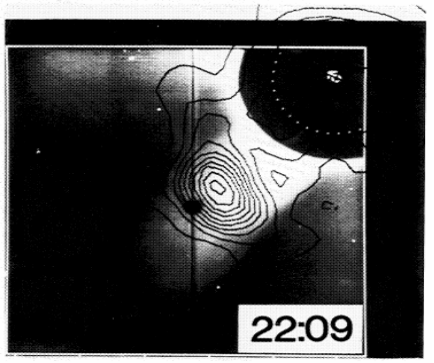

Soft X-ray light curve, TypeII T_B(A), TypeIV T_B(B,C), height-time plot of Moving Type IV; TypeIV contours at 2035 & 2209 UT superposed on disrupting streamer.

CME –associated TypeII, TypeIV locations. Schematic Model

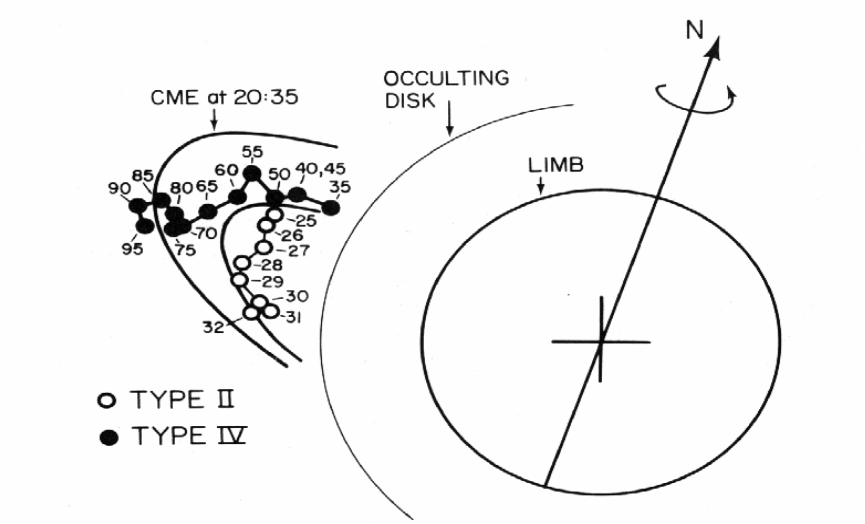

FIG. 3.—Motion of the centroids of moving type IV and type II bursts, relative to the 20:35 UT image of the CME. The type II centroids are plotted every minute, and the moving type IV centroids are plotted every 5 minutes. The labels on the centroids represent the times in minutes after 20:00 UT; e.g., 75 means 21:15 UT. The last three moving type IV centroids are corrected for ionospheric refraction using the quiet-Sun radio features.

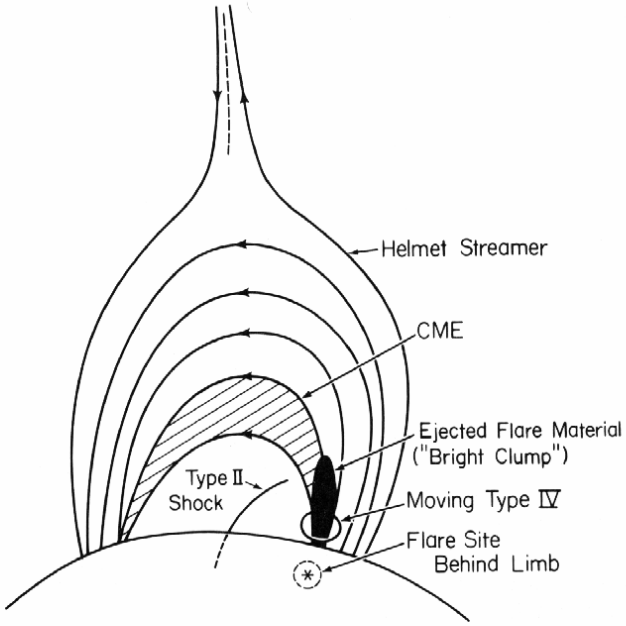

FIG. 7.—Schematic model showing the relation of the radio bursts and the mass ejection event. The direction of the type II shock is indicated. The moving type IV burst is supposed to be located on the heated prominence material ejected from a flare. Asterisk (*) denotes the location of flare behind the limb. The helmet streamer disrupts later, and the material moves outward, with the legs separating.

A Fast CME in radio

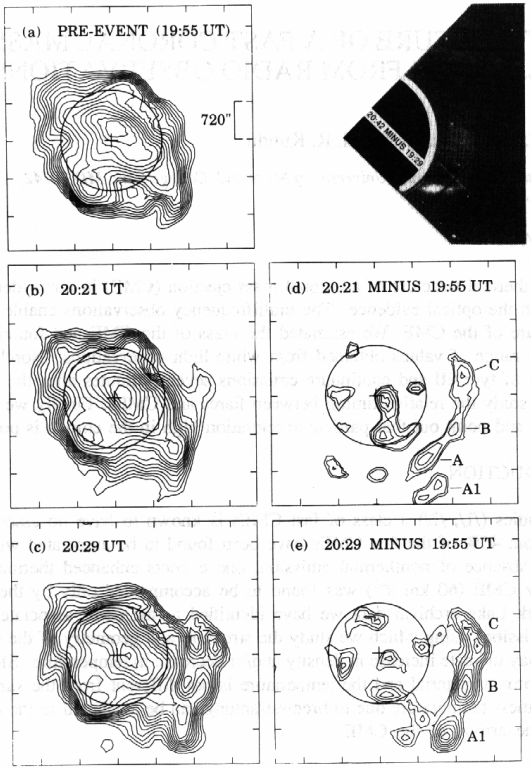

Fig. 1. Radio maps of the Sun at (a) 19:55, (b) 20:21 and (c) 20:29 UT and the difference maps at (d) 20:21 and (e) 20:29 UT, showing the arrival of the CME at the 73.8 MHz plasma level. The 19:55 (pre-event) map is used for subtraction. The white light CME (SMM-C/P) at 20:42 UT is shown in the right hand top corner. C is the northernmost feature discussed in the text. A, A1 and B are other clumps in the radio CME.

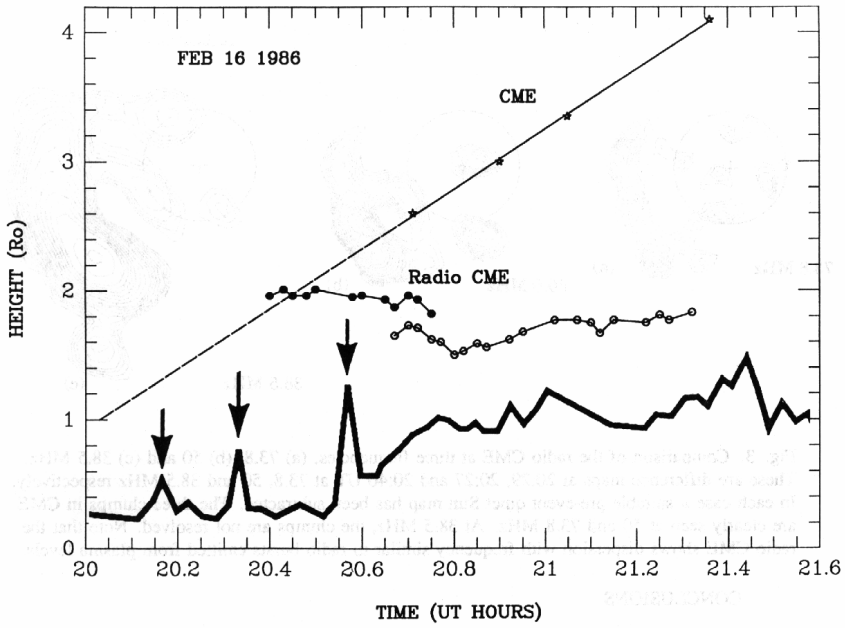

Fig. 2. Height – time plot of the white light CME, radio CME and the nonthermal continuum. The brightness temperature variation is shown at the bottom. The spikes marked by arrows are type III bursts. The rise in brightness after the type III's is due to the nonthermal continuum.

The fast radio CME and production of radio-emitting electrons (schematic)

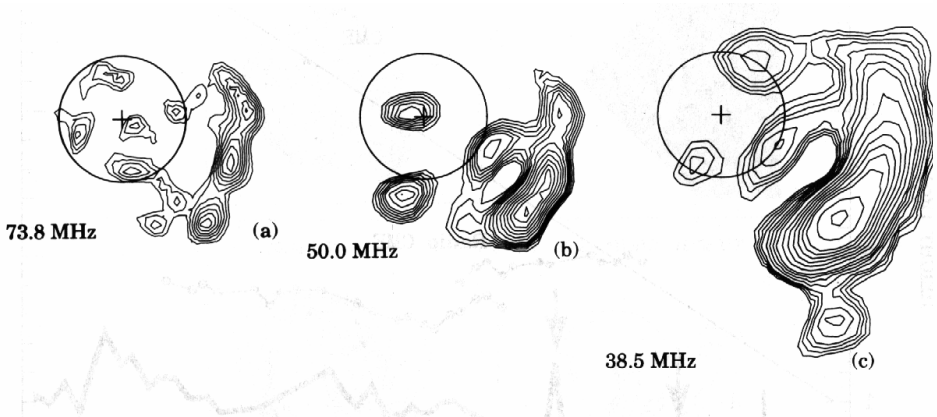

Fig. 3. Comparison of the radio CME at three frequencies, (a) 73.8, (b) 50 and (c) 38.5 MHz. These are difference maps at 20:29, 20:27 and 20:40 UT at 73.8, 50 and 38.5 MHz respectively. In each case a suitable pre-event quiet Sun map has been subtracted. The three clumps in CME are clearly seen at 50 and 73.8 MHz. At 38.5 MHz, the clumps are not resolved. Note that the radio CME shows dispersion with frequency similar to radio bursts emitted from plasma levels.

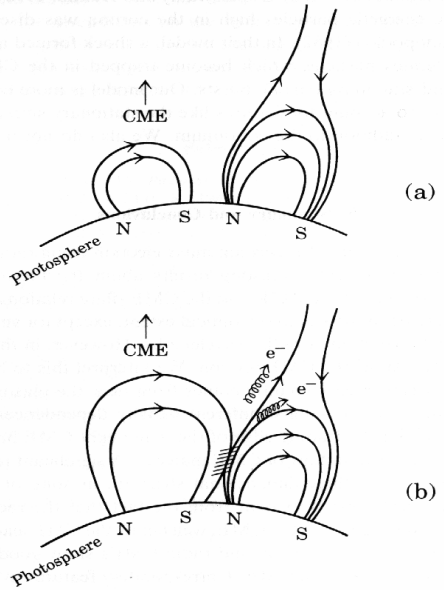

Fig. 8. Schematic model illustrating the possibility of particle acceleration high in the corona due to the motion of the CME pressing against the oppositely directed magnetic field structure. (a) Early in the event when the CME and the streamer structure are well separated. (b) Later during the event when the CME expands and comes in contact with the neighboring streamer structure. Particle acceleration occurs at the hatched region and the particles propagate along open and closed field lines. Propagation along open field lines produce the type III bursts, and those trapped in closed field lines produce the continuum emission.

Stellar astronomy: Doing science while Partying

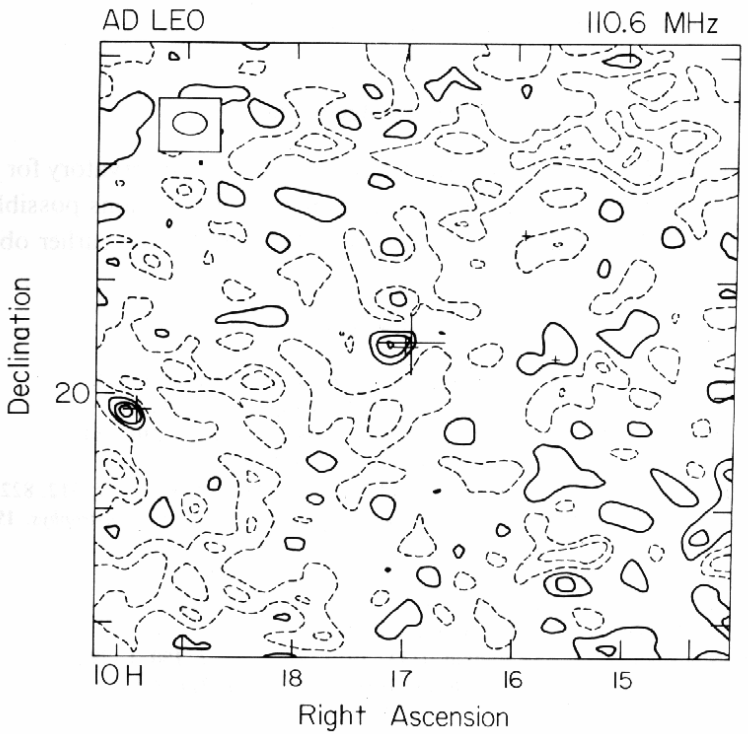

Fig. 3. Map of the area around AD Leo for all the data on December 15, 1985. The contour levels are: −1.5, −0.9, −0.3, +0.5, +1.1, and +1.7 Jy. The extragalactic source 1017+201 is clearly shown as a possible extension towards the position of AD Leo. The map has been corrected for ionospheric refraction.

SIRA-Related Remarks

- TypeIII, TypeIII Storms, Relation to solar active region and related Physics
- Extension of coronal streamer density as far as you can go- beyond 30 Ro up to 1/3 AU?
- Coronal Holes – same comment- unknown what will be seen
- CME will clearly be seen- along with IP type II? Relationship of near-sun typeII with IP typeII.
- Properties of type IV far from Sun